RSC Advances

PAPER

View Article Online
View Journal | View Issue

Cite this: *RSC Adv.*, 2017, **7**, 20241

Phase stability, elastic and electronic properties of Hf–Rh intermetallic compounds from first-principles calculations

Mingliang Wang,[ab] Cunjuan Xia,[a] Yi Wu,[a] Dong Chen,*[a] Zhe Chen,*[b] Naiheng Ma[b] and Haowei Wang[ab]

Received 17th February 2017
Accepted 27th March 2017

DOI: 10.1039/c7ra01976a

rsc.li/rsc-advances

The phase stability, elastic and electronic properties of binary Hf–Rh compounds have been studied using first-principles calculations based on density functional theory. The equilibrium lattice constants, formation enthalpies, elastic constants, and elastic moduli are presented. Among the binary Hf–Rh compounds, Hf_3Rh_5 is the most stable with the lowest formation enthalpy. For the equiatomic HfRh phase, it tends to crystallize in the ZrIr-type structure, followed by $L1_0$, and then B2 at the ground state based on the analysis of formation enthalpies. Therefore, the crystal structure of the lower temperature HfRh phase is suggested to be the ZrIr-type. This conclusion is in agreement with the experimental reports in the literature. Besides, Hf_3Rh_4 are proposed to be the Pu_3Pd_4-type for the first time. Furthermore, our calculated elastic constants for Hf_2Rh, ZrIr-HfRh, $L1_0$-HfRh, B2-HfRh, Hf_3Rh_4, Hf_3Rh_5 and $HfRh_3$ can all satisfy the Born criteria, indicating their mechanical stabilities. When ZrIr-HfRh is adopted, the bulk modulus (B) increases linearly with the growing Rh atomic concentration. Meanwhile, Young's modulus linearly increases with growing shear modulus, and the compound with a higher Poisson's ratio owns a higher B/G ratio simultaneously. Overall, the results also indicate that all the considered Hf–Rh compounds should be ductile. Finally, the electronic structure is analyzed to understand the essence of structural stability of the binary compound.

1. Introduction

Among the platinum group metals, Rh has the smaller density and better oxidation resistance with a high melting temperature, ensuring it as a promising candidate for industry applications such as developing refractory superalloys.[1] During the past decades, Rh-based alloys have received great research interest due to these properties among all the metals, *e.g.* high melting temperature, the highest corrosion resistance and high strength.[2] Meanwhile, Hf is used extensively as an alloying element in transition metal-based superalloys, which are designed to withstand high temperatures and pressures. Hf is a useful addition to transition metals, in which it can form the second phase to improve a material's strength under extreme conditions.[3] The investigations on Hf–Rh systems should be of critical importance, which has attracted attention with respect to the superalloys,[4–6] the occurrence of superconductivity,[7] the amorphization behavior[8] and the electrocatalytic hydrogen production ability[9] of Hf–Rh alloys.

The Hf–Rh phase diagram was studied by Waterstrat *et al.*,[10] and suggested the existence four types of binary compounds, *i.e.*, Hf_2Rh, HfRh, Hf_3Rh_5 and $HfRh_3$. Lately, Eremenko *et al.*[11] reassessed this diagram, and reported seven intermediated phases in this system, including Hf_2Rh, HfRh (with three types of polymorphs), Hf_3Rh_4, Hf_3Rh_5 and $HfRh_3$. Based on published results,[10–15] Okamoto *et al.*[16] has reviewed the Hf–Rh phase diagram, and determined the crystal structure of several binary Hf–Rh compounds. Hf_2Rh and Hf_3Rh_5 should form peritectically at 1723 K and 2168 K and have Ti_2Ni- and Ge_3Rh_5-type structures, respectively. Besides, $HfRh_3$ has a cubic $L1_2$ type structure, and can melt congruently at 2278 K at the stoichiometric composition. In addition, the equiatomic HfRh phase has a more complex situation. Initially, the high temperature δ (B2) HfRh phase is confirmed, and should melt congruently at 2453 K at the stoichiometric composition. Secondly, the δ' ($L1_0$) HfRh phase is proposed to be stable at medium temperature from ~873 K to 973 K. Still, there is a low temperature δ'' HfRh phase existing below ~873 K without informing of the crystal structure. The similar situation has also occurred in Hf_3Rh_4, which should form peritectically at 1718 K and lack of structure information.

Although the Hf–Rh system has been studied for a long time, it is believed that the systematically theoretical study on Hf–Rh system discussing and revealing the crystal structure to the

[a]State Key Laboratory of Metal Matrix Composites, Shanghai Jiao Tong University, China. E-mail: chend@sjtu.edu.cn

[b]School of Materials Science & Engineering, Shanghai Jiao Tong University, No. 800 Dongchuan Road, Shanghai 200240, China. E-mail: zhe.chen@sjtu.edu.cn; Tel: +86-21-54747597

unknown HfRh and Hf_3Rh_4 phases has been eluded. Also, the experimental studies are also limited. The reliable information, such as formation enthalpies, and elastic properties (*i.e.*, elastic constant, and bulk/shear/Young's modulus) are lacking. Intensive studies are also required to clarify the phase and mechanical stability and the properties of the binary compounds. Therefore, a comprehensive investigation of the ground-state phase stability, elastic and electronic properties of Hf–Rh compounds using first-principles calculations based on the density functional theory (DFT) has been performed in this work. In Section 2, the computational strategies are presented in detail. The calculated results are discussed and compared with the available experimental and theoretical results in Section 3. Finally, the conclusions are summarized in Section 4.

2. Computational methods

All theoretical calculations were carried out by a first-principles plane-wave pseudopotential method based on DFT through the CASTEP package[17] in the current work. The ultrasoft pseudopotential was used to model the ion–electron interaction.[18] The generalized gradient approximation (GGA) with the Perdew–Burke–Ernzerhof (PBE) exchange–correlation functional was utilized.[19–21] The states of $Hf5d^26s^2$ and $Rh4d^85s^1$ were taken as the basis set in the calculations. The kinetic cutoff energy for plane waves was settled at 400 eV. The special points sampling integration over the Brillouin zone was employed by using the Monkhorst–Pack method[22] with determined *k*-point separation of 0.02 $Å^{-1}$ in three lattice directions for each structure. The Pulay scheme of density mixing was applied for the evaluation of energy and stress.[23,24] The optimization of atom coordinates and lattice constants were made by minimization of the total energy. The Broyden–Fletcher–Goldfarb–Shanno (BFGS) minimization scheme was used in the geometry optimization.[25] The tolerances of the geometry optimization were set as follows: the difference of the total energy within 0.001 eV per cell, maximum ionic force within 100 eV $Å^{-1}$, maximum ionic displacement with in 100 Å, and maximum stress within 100 GPa. The calculation of total energy and electronic structure were followed by cell optimization with SCF tolerance of 1.0×10^{-4} eV per cell. The total energies and the density of states (DOS) under the optimized structures were calculated by means of the corrected tetrahedron Blöchl method.[26]

From the view of thermodynamics, the formation enthalpy (H_f) is defined as the total energy difference between the compound and its constituents in proportion to the composition. The formation enthalpy (H_f) is calculated by the following equation:

$$H_f = \frac{1}{a+b}\left(E_{total} - aE^{Hf}_{solid} - bE^{Rh}_{solid}\right) \quad (1)$$

where E_{total} is the total energy of the unit cell, a (or b) is the atom number of Hf (or Rh) in a unit cell, and E^{Hf}_{solid} (or E^{Rh}_{solid}) is the energy per Hf (or Rh) element in the solid state of the crystal structure. During the calculation for E^{Hf}_{solid} and E^{Rh}_{solid}, Hf and Rh are HCP and FCC structure, respectively. The formation enthalpy (H_f) is used to evaluate the thermodynamic stability of the compound. The lower H_f value represents the better thermodynamic stability.

3. Results and discussion

3.1 Crystal structure and stability

Based on the former studies, five chemical compositional Hf_x-Rh_y compounds (*i.e.*, Hf_2Rh, HfRh, Hf_3Rh_4, Hf_3Rh_5 and $HfRh_3$) are adopted. The Ti_2Ni-type Hf_2Rh, Ge_3Rh_5-type Hf_3Rh_5, and $L1_2$-$HfRh_3$ are used in accordance with the experimental observations. The optimized lattice constants for these compounds are listed in Table 1, along with published lattice constants for comparison from experimental (Ti_2Ni-type Hf_2Rh,[27] Ge_3Rh_5-type Hf_3Rh_5,[28] $L1_2$-$HfRh_3$ (ref. 29)) and theoretical (Ti_2Ni-type Hf_2Rh[9] and $L1_2$-$HfRh_3$ (ref. 4, 5 and 30)) results at the ground state. For these three compounds, the differences between the optimized and experimental lattice constants are small accordingly. Thus, the reliability of our calculation method and the chosen parameters have been confirmed, which also assure the credibility of subsequent results.

For HfRh, Ramam *et al.*[14] reported the $L1_0$-HfRh was stable at lower temperature, and B2 HfRh was observed at higher temperatures experimentally. Waterstrat *et al.*[10] confirmed the existence of B2 HfRh, and also reported the occurrence of "tetragonally distorted" B2 phase ($Hf_{46}Rh_{54}$, $a = 3.268$ Å, $c = 3.150$ Å; $Hf_{45}Rh_{55}$, $a = 3.12$ Å, $c = 3.418$ Å). Such phase was ascribed to the $L1_0$-HfRh in the Hf–Rh phase diagram generalized by Okamoto.[16] In addition, Waterstrat *et al.*[10] also considered the possible formation of HfRh phase in the ZrIr-type[12] and/or NbRu-type ($Hf_{42}Rh_{58}$: $a = 4.392$ Å, $b = 4.306$ Å, $c = 3.470$ Å (ref. 12)) crystal structures.

About the ZrIr-type structure, an earlier X-ray diffraction (XRD) study suggested the ZrIr-type compound may have either B27 or B33 structure.[31] In disagreement with this analysis, Semenova *et al.*[32] identified the structure as a monoclinic TiNi (B19′)-type. However, Waterstrat *et al.*[33] considered that the ZrIr-type compound should be a new orthorhombic structure that was resembling to the $DyGe_3$ structure. Stalick *et al.*[34] agreed this idea and determined the crystal structure of orthorhombic ZrIr compound using powder neutron diffraction data. Through first-principles calculations, Chen *et al.*[35] theoretically computed the structural properties of ZrIr compound with the B19′, B27, B33 and ZrIr-type (from ref. 34) structures, and found the calculated lattice constants of ZrIr-type phase were in good agreement with the available experimental results. Therefore, the crystal information of the original ZrIr-type phase is adopted from ref. 34.

Regarding the NbRu-type structure, it is suggested to be an orthorhombic structure.[36–41] However, its crystal structure has ever reached consensus yet. For example, Mitarai *et al.*[39] studied the crystal structure of NbRu-type IrTi using XRD analysis experimentally and refined the structure with *ab initio* calculation theoretically. They proposed that the NbRu-type structure has space group *Cmmm* (65), and the atomic positions: Nb (1) 0.0 0.5 0.0, (2) 0.5 0.0 0.0; Ru (1) 0.0 0.0 0.5, (2) 0.5 0.5 0.5. Shao *et al.*[40] discussed the structural, thermodynamic and elastic

Table 1 Structural information and optimized lattice constants and available experimental and theoretical values, and the formation enthalpy (H_f) binary Hf–Rh compounds

	Composition (at% Rh)	Prototype	Structure	a (Å)	b (Å)	c (Å)	H_f (eV per (atom))
Hf_2Rh	33.3	Ti_2Ni	*Fd3ms*(227)	12.4719			−0.6538
				12.317[a]			−0.64[b]
				12.334[c]			
HfRh	50	ZrIr	*Cmcm*(63)	3.3695	19.8796	4.442	−0.9225
		$L1_0$	*P4/mmm*(123)	3.309889		3.309942	−0.9059
	54			3.268[d]		3.15[d]	−0.9539[e]
	55			3.12[d]		3.41[d]	
		B2	*Pm3m*(221)	3.3088			−0.9015
				3.227[f]			−0.9506[e]
				3.284[g]			−0.996 ± −0.0229[h]
		NbRu([39])	*Cmmm*(65)	4.6436	4.6437	3.3632	−0.8996
	58			4.392[d]	4.306[d]	3.470[d]	
		B27	*Pnma*(62)	6.0941	4.5237	5.4062	−0.8994
							−0.899[i]
		B33	*Cmcm*(63)	3.2007	10.2247	4.5364	−0.8826
							−0.9433[e]
		B19	*Pmma*(51)	4.6972	3.1307	4.9632	−0.8789
							−0.9402[e]
		B11	*P4/nmms*(129)	3.6268		5.8085	−0.6742
Hf_3Rh_4	57.1	Pu_3Pd_4	*R3h*(148)	12.3285		5.6375	−0.9284
		Ta_3B_4	*Immm*(71)	3.2002	18.2383	4.3887	−0.669
		Ti_3Cu_4	*I4/mmm*(139)	3.4118		21.8902	−0.6099
		C_3Al_4	*R3mh*(166)	4.6972		24.7277	−0.2027
		Co_3S_4	*Fd3ms*(227)	11.0626			0.2877
		Th_3P_4	*I43d*(220)	8.2242			27.8134
Hf_3Rh_5	62.5	Ge_3Rh_5	*Pbam*(55)	5.5919	10.7064	4.2877	−0.9344
				5.58[j]	10.73[j]	4.25[j]	−0.9280[i]
$HfRh_3$	75	$L1_2$	*Pm3m*(221)	4.007			−0.791
				3.912[k], 3.942[e]			−0.891[e]
				3.94[l], 3.86[l]			−0.762[i]
				3.95[m]			

[a] Experimental values from ref. 27. [b] Theoretical values from ref. 46. [c] Theoretical values from ref. 9. [d] Theoretical values from ref. 10. [e] Theoretical values from ref. 30. [f] Experimental values from ref. 47. [g] Theoretical values from ref. 48. [h] Experimental values from ref. 49. [i] Theoretical values from ref. 44. [j] Experimental values from ref. 28. [k] Experimental values from ref. 29. [l] Theoretical values from ref. 5. [m] Theoretical values from ref. 4.

properties of NbRu, and found the *Pnma* (62)/B27 NbRu structure was both thermodynamically and mechanically stable at the ground state. As a result, both *Cmmm* (65) and *Pnma* (62) structures are used for structural optimization in this work. The obtained equilibrium lattice constants for *Cmmm* (65) HfRh and *Pnma* (62) HfRh are shown in Table 1. Clearly, the *Cmmm* (65) HfRh is more approaching to the experimentally reported NbRu-type HfRh ($Hf_{42}Rh_{58}$: $a = 4.392$ Å, $b = 4.306$ Å, $c = 3.470$ Å (ref. 12)), indicating that *Cmmm* (65) NbRu structure is more probable.

Resultantly, the HfRh is theoretically inclined to form the crystal structure in the following sequence of ZrIr-type > $L1_0$ > B2 > B27 > B33 > B19 > B11 structures based on the H_f values. Our results show good accordance with the experimental observations. For instance, Okamoto *et al.*[16] generalized Hf–Rh phase diagram based on the available experimental data, and concluded there were three phases for equiatomic HfRh, including the high temperature δ (B2) phase, medium temperature δ' ($L1_0$) phase, and low temperature unknown δ'' phase. Basically, the lower temperature phase at the ground state should possess the more negative H_f value.[42,43] Therefore, the H_f values for HfRh phases are in the order of δ'' > $L1_0$ > B2 structures. Theoretically, Xing *et al.*[30] suggested the thermodynamic stability of HfRh was in the order of B33 > $L1_0$ > B2 > B19 structure. However, the B33 structure phase has ever reported for HfRh. Similarly, Levy *et al.*[44] considered the *Pnma* (B27) HfRh should be more stable than the B2 type, where they did not provide lattice constants for evaluation. Nevertheless, we have proved *Pnma* (B27) HfRh is less possible to form as the NbRu-type structure (Table 1). Conclusively, it is suggested that the unknown δ'' phase at low temperature should be ZrIr-type, which also corresponds to Waterstrat's work,[10] and the HfRh phases are able to crystallize in the order of ZrIr-type > $L1_0$ > B2 structures.

For Hf_3Rh_4, the Pu_3Pd_4-, Ta_3B_4-, Ti_3Cu_4-, C_3Al_4-, Co_3S_4-, Th_3P_4-type structure are considered. Co_3S_4- and Th_3P_4-type Hf_3Rh_4 are unlikely to more due to their positive H_f values. The Pu_3Pd_4-type Hf_3Rh_4 should be the favored crystal structure with the most negative H_f value. This is similar to Zr_3Rh_4 which also possesses the Pu_3Pd_4-type structure.[45]

Fig. 1 exhibits the convex hull plot of the formation enthalpies of binary Hf–Rh compounds calculated at the ground state, along with the theoretical values from Levy's work,[44] Miedema's model,[50] Koteski's work[46] and Xing's work,[30] and experimental values from Guo's work[49] and Gachon's work.[51] For Hf_2Rh, our calculated value is −0.6538 eV per atom, agreeing well with the experimental value of −0.6934 ± −0.0156 eV per atom (ref. 51) and theoretical value of −0.64 eV per atom.[46] About $HfRh_3$, our calculated value is −0.791 eV per atom, which is in good accordance with the theoretical value of −0.762 eV per atom (ref. 44) and −0.891 eV per atom.[30] All these values are a bit larger than the experimental value of −0.6063 ± −0.0125,[51] although this experimental value is based on the phase $Rh_{0.79}Hf_{0.21}$. In addition, the enthalpies of formation of HfRh, Hf_3Rh_4 and Hf_3Rh_5 at their respective ground-state phases fall on a common straight line, implying that the concentrations ranges for different compounds are quite narrow. Comparably, the convex hull plot of Miedema's model[50] shows the lowest point of H_f values at the HfRh phase. However, the convex hull plots of this theoretical work, Levy's theoretical work[44] and Gachon's experimental work[49] have complied well with each other, and exhibited the similar contours, where the Hf_3Rh_5 compound has the most negative H_f value, signifying it is the most stable phase among binary Hf–Rh compounds.

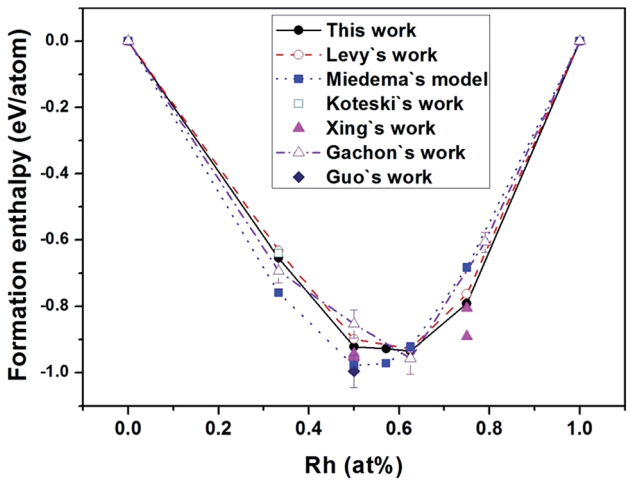

Fig. 1 The convex hull plot of the formation enthalpies of binary Hf–Rh compounds calculated at the ground state in comparison with the experimental values from Gachon's work[51] and Guo's work,[49] and theoretical values from Levy's work,[44] Miedema's model,[50] Koteski's work[46] and Xing's work.[30] The tie-line in each work has joined the low enthalpy structures at the vertices of the convex hull.

3.2 Mechanical properties

To investigate the mechanical stability and elastic properties, the single-crystal elastic constants of the binary Hf–Rh phases, as well as pure Hf and Rh, are calculated by the stress–strain method[52,53] at their optimized structures. To calculate the elastic constant (C_{ij}), a deformed cell is introduced. The elastic strain energy is presented as following:[54]

$$U = \frac{\Delta E}{V_0} = \frac{1}{2}\sum_{i}^{6}\sum_{j}^{6} C_{ij}e_i e_j \quad (2)$$

where ΔE is the energy difference; V_0 is the volume of unit cell; C_{ij} ($i,j = 1, 2, 3, 4, 5$ and 6) is the elastic constant; e_i and e_j are the applied strains.

Using the stress–strain methods, the single-crystal elastic constants for seven Hf–Rh binary intermetallics and pure Hf and Rh metals have been derived and summarized in Table 2, in comparison with the available experimental and theoretical values. For pure Hf and Rh metals, our calculated elastic constants are in good agreement with experimental[55,56] and theoretical[4] values. It has thus indicated the calculation method adopted in the work is effective to predict the elastic properties of metallic compounds. For $HfRh_3$, the derived elastic constants are in good agreement with the available theoretical values.[4] However, the experimental and theoretical elastic constants for other six Hf–Rh compounds are not available to the best of our

Table 2 The obtained single-crystal elastic constant (C_{ij}, GPa) along with the experimental and theoretical values for binary Hf–Rh compounds and pure Hf/Rh metals

Compound	C_{11}	C_{22}	C_{33}	C_{44}	C_{55}	C_{66}	C_{12}	C_{13}	C_{23}	C_{14}	C_{15}
Hf	193.5		205.2	56.4			82.7	77.2			
Ref. 55 (exp. values)	181.0		197.0	55.7			77.0	66.0			
Hf_2Rh	245.6			55.8			125.3				
HfRh (ZrIr)	243.7	277.9	277.6	85.7	92.5	60.6	135.5	161.1	132.4		
HfRh ($L1_0$)	234.0		232.8	69.0		69.1	165.7	165.4			
HfRh (B2)	234.6			69.4			165.9				
Hf_3Rh_4	292.3		313.4	27.9			157.3	130.9		−17.7	26.3
Hf_3Rh_5	330.8	304.6	301.2	96.1	85.1	47.6	116.2	149.8	168.0		
$HfRh_3$	330.4			144.5			170.0				
Ref. 4 (theo. values)	296.0			140.0			158.0				
Ref. 5 (theo. values)	319.0			144.0			163.0				
Rh	394.7			171.7			183.6				
Ref. 55 (exp. values)	413.0			184.0			194.0				
Ref. 56 (exp. values)	416.0			184.0			197.0				
Ref. 4 (theo. values)	386.0			171.0			172.0				

knowledge. Therefore, our calculated elastic constants for Hf_2Rh, ZrIr-HfRh, $L1_0$-HfRh, B2-HfRh, Hf_3Rh_4 and Hf_3Rh_5 compounds should provide useful data for comparison in future experimental and theoretical studies.

In order to evaluate the phase stability of the compound, the mechanical stability is analyzed in combination of the elastic constant and Born's stability criteria.[57] For a stable crystalline structure, the elastic constant should satisfy the Born's criteria to prove its mechanical stability. In terms of seven binary Hf–Rh intermetallics considered in this work, Hf_2Rh, B2-HfRh, and $HfRh_3$ are ascribed to the cubic structure, ZrIr-HfRh and Hf_3Rh_5 have the orthorhombic structure, and Hf_3Rh_4 and $L1_0$-HfRh possess the trigonal and tetragonal structure, respectively.

For the cubic crystal, there are three independent elastic constants. The mechanical stability criteria are provided in the following equation:[58,59]

$$C_{11} > 0;\ C_{44} > 0;\ C_{11} > |C_{12}|;\ C_{11} + 2C_{12} > 0 \quad (3)$$

In Table 2, the elastic constants of the cubic Hf_2Rh, B2-HfRh, and $HfRh_3$ crystals can satisfy the above criteria accordingly, confirming their mechanically stability.

Regarding the orthorhombic phase, it has nine independent elastic constants, and the restrictions of mechanical stability for are presented the following equation:

$$C_{11} > 0;\ C_{22} > 0;\ C_{33} > 0;\ C_{44} > 0;\ C_{55} > 0;\ C_{66} > 0;\ C_{11} + C_{22} + C_{33} + 2(C_{12} + C_{13} + C_{23}) > 0;\ C_{11} + C_{22} - 2C_{12} > 0;\ C_{11} + C_{33} - 2C_{13} > 0;\ C_{22} + C_{33} - 2C_{23} > 0 \quad (4)$$

It is seen that the elastic constants for ZrIr-HfRh and Hf_3Rh_5 can both meet the restrictions of mechanical stability, implying both compounds are mechanically stable.

About the trigonal Hf_3Rh_4 phase with seven independent elastic constants, the mechanical stability criteria are included in the following formula:[60]

$$C_{11} > 0;\ C_{33} > 0;\ C_{44} > 0;\ C_{11} > |C_{12}|;\ (C_{11} + C_{12})C_{33} - 2{C_{13}}^2 > 0;\ (C_{11} - C_{12})C_{44} - 2{C_{14}}^2 > 0 \quad (5)$$

Clearly, all the elastic constants of Hf_3Rh_4 exhibited in Table 2 can satisfy Born's criteria for mechanical stability.

For the tetragonal crystal, the stability criteria are shown in the following formula:[61]

$$C_{11} > 0;\ C_{33} > 0;\ C_{44} > 0;\ C_{66} > 0;\ C_{11} - C_{12} > 0;\ C_{11} + C_{33} - 2C_{13} > 0;\ 2(C_{11} + C_{12}) + C_{33} + 4C_{13} > 0 \quad (6)$$

Through the validation of the formula (6), the $L1_0$-HfRh phase has six independent elastic constants to ensure its mechanical stability.

Conclusively, the seven Hf–Rh intermetallics considered, *i.e.*, Hf_2Rh, ZrIr-HfRh, $L1_0$-HfRh, B2-HfRh, Hf_3Rh_4, Hf_3Rh_5 and $HfRh_3$, are all suggested mechanically stable.

The elastic constants C_{11} and C_{33} should characterize the x direction and z direction resistances to linear compression, respectively.[62,63] In Table 2, the ZrIr-HfRh and Hf_3Rh_4 have larger C_{33} values, indicating their higher incompressibility under the z direction uniaxial stress. In Hf_3Rh_5, it is more compressible along z direction than that along x direction due to the larger C_{11} value. In the case of C_{44}, it is interpreted as the resistance to monoclinic shear in the (100) plane, and is the critical parameter relating to the shear modulus.[64,65] In Table 2, the largest C_{44} for $HfRh_3$ has suggested that $HfRh_3$ has the strongest resistance to shear in the (100) plane, while Hf_3Rh_4 has the smallest C_{44} to show the weakest resistance to shear in the (100) plane.

Based on the single-crystal elastic constant, three types of algorithms corresponding to different bounds are adopted to estimate elastic properties of polycrystalline materials. In detail, the Voigt[66]/Reuss[67] method is the larger/smaller value of the actual effective modules on the assumption of uniform strain/stress imposed on the polycrystalline structure. For the cubic structure, the upper and the lower bounds for the bulk (B) and shear (G) modulus related to Voigt and Reuss methods are exhibited in the formula (7-1) to (7-3):[59]

$$B_V = B_R = \frac{1}{3}(C_{11} + 2C_{12}) \quad (7\text{-}1)$$

$$G_V = \frac{1}{5}(C_{11} - C_{12} + 3C_{44}) \quad (7\text{-}2)$$

$$G_R = \frac{5(C_{11} - C_{12})C_{44}}{4C_{44} + 3(C_{11} - C_{12})} \quad (7\text{-}3)$$

Furthermore, the equations used to compute the upper and the lower bounds for the bulk and shear modulus with orthorhombic, trigonal and tetragonal structures can be referred to the ref. 60, 61 and 42, accordingly.

In addition, the arithmetic average of Voigt and Reuss bounds is termed as the Voigt–Reuss–Hill (VRH) method.[68] Using the VRH averaging method, the bulk modulus (B) and shear modulus (G) are calculated in the eqn (8):

$$B = \frac{1}{2}(B_R + B_V) \quad (8\text{-}1)$$

$$G = \frac{1}{2}(G_R + G_V) \quad (8\text{-}2)$$

Young's modulus (E) and Poisson's ratio (ν) are also major elasticity related parameters, which can be calculated using the following formula:

$$E = \frac{9BG}{3B + G} \quad (9\text{-}1)$$

$$\nu = \frac{3B - 2G}{2(3B + G)} \quad (9\text{-}2)$$

The calculated polycrystalline bulk modulus, shear modulus, Young's modulus, Poisson's ratio and B/G values for seven Hf–Rh compounds and pure Hf/Rh metals using VRH methods are calculated and tabulated in Table 3. For pure Hf and Rh metals, the obtained elastic properties are in good agreement with the

published experimental[55,56] and theoretical[4] values, validating the precision of the predicted elastic properties of metallic materials.

The bulk modulus is a measure of resistance to volume change under external pressures. From Table 3, it is observed that the $HfRH_3$ has the strongest resistance to volume change by applied pressure, while Hf_2Rh owns the smallest. In addition, the bulk modulus has also been deem as the measure of the average bond strength of atoms for the given crystal.[69] Among binary Hf–Rh intermetallics, $HfRH_3$ is suggested have the strongest average bond strength of atoms, and Hf_2Rh should be the weakest one. In addition, the B2- and $L1_0$-HfRh phases have the similar bulk moduli, and both are a bit larger than the ZrIr-HfRh (Table 3). For Hf_2Rh, B2-HfRh and $HfRh_3$, the calculated bulk moduli are in good agreement with those theoretical values for Hf_2Rh (Cavor's work[9]), B2-HfRh (Novakovic's work[48]), and $HfRh_3$ (Chen's[4] and Surucu's[5] work), accordingly. Notably, the theoretical bulk modulus for $HfRh_3$ reported by Rajagopalan[70] is much larger than other available values, which requires further scrutinizing.

When ZrIr-type HfRh is considered, the relationship between bulk modulus and atomic concentration of Rh has been exhibited in Fig. 2. It is seen that the bulk moduli of Hf–Rh compounds are linearly rising with the increasing Rh atomic concentration (at%), and the fitting line is $y = 117.96 + 1.357x$ with $R^2 = 0.9961$. It is noteworthy that the R^2 is quite small to assure the precision of the fitted relationship.

The shear modulus is a measure of resistance to reversible deformations over the shear stress. In Table 3, the $HfRH_3$ has the strongest resistance to reversible deformations over the shear stress, and Hf_3Rh_4 possesses the smallest among Hf–Rh compounds. Furthermore, the B2- and $L1_0$-HfRh phases have the similar shear moduli, and both are smaller than the ZrIr-HfRh (Table 3). Regarding the Young's modulus, it represents

Table 3 The polycrystalline bulk modulus (B), shear modulus (G), Young's modulus (E), Poisson's ratio (ν), and B/G ratio for binary Hf–Rh compounds and pure Hf/Rh metals deduced from the VRH method

Compound	B (GPa)	G (GPa)	E (GPa)	ν	B/G
Hf	118.5	57.2	147.9	0.292	2.070
Ref. 55 (exp. values)	108.5	55.8	142.9	0.280	1.944
Hf_2Rh	165.4	57.5	154.5	0.344	2.877
Ref. 40 (theo. values)	148.7				
HfRh (ZrIr)	183.8	70.5	187.5	0.330	2.609
HfRh ($L1_0$)	188.2	52.0	142.7	0.374	3.622
HfRh (B2)	188.8	52.3	143.7	0.373	3.61
Ref. 48 (theo. values)	173.0				
Hf_3Rh_4	192.9	39.3	110.3	0.405	4.913
Hf_3Rh_5	200.3	76.2	202.8	0.331	2.629
$HfRh_3$	223.5	114.1	292.5	0.282	1.959
Ref. 4 (theo. values)	204.0	105.4	269.7	0.280	1.936
Ref. 5 (theo. values)	215.0	112.6	287.6	0.277	1.910
Ref. 70 (theo. values)	274.8				
Rh	254.0	141.2	357.5	0.265	1.798
Ref. 55 (exp. values)	267.0	149.4	377.8	0.264	1.787
Ref. 56 (exp. values)	270.0	149.4	378.4	0.266	1.807
Ref. 4 (theo. values)	243.3	141.7	356.0	0.256	1.717

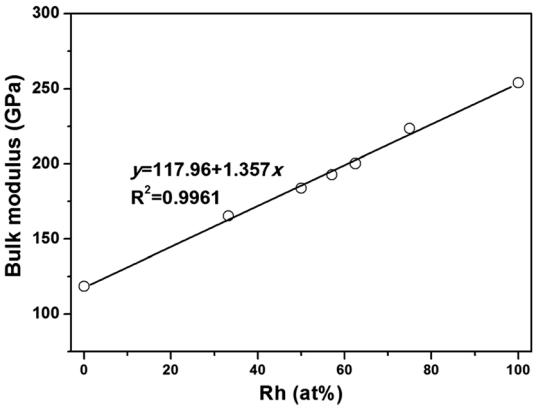

Fig. 2 The calculated bulk modulus (B) *versus* atomic concentration of Rh for the binary Hf–Rh compounds.

the stiffness of materials. Overall, $HfRH_3$ owns the largest, and Hf_3Rh_4 has the smallest Young' modulus among the Hf–Rh compounds (Table 3). It means $HfRH_3$ and Hf_3Rh_4 are the most and least stiffest phases among binary Hf–Rh intermetallics, respectively. Besides, the ZrIr-HfRh has the larger Young's modulus than both B2- and $L1_0$-HfRh phases (Table 3). Generally, the calculated shear and Young's moduli are both in well compliance with those theoretical values for $HfRh_3$ (Chen's[4] and Surucu's[5] works).

The obtained shear modulus and Young's modulus are depicted as a function of Rh atomic concentration in Fig. 3a and b, respectively. Since there is not explicit relationship shown in each figure, the connecting lines are only used as the guide for observation in both figures. However, the variations of shear modulus (Fig. 3a) and Young's modulus (Fig. 3b) have exhibited the similar tendencies with increasing Rh concentration, if the ZrIr-HfRh is selected. Therefore, the relationship between shear modulus (G) and Young's modulus (E) has been constructed, as shown in Fig. 3c, showing that E has linearly increased with the growing G. The linear relation can be formulated as $E = 13.523 + 2.443G$. Clearly, the R^2 of the fitted line is 0.9989, which implies good relationship between these two factors.

Poisson's ratio (ν) is used to quantify the stability of the crystal against shear deformation, which usually ranges from −1 to 0.5.[71–73] The larger Poisson ratio signifies the better plasticity in materials. The Poisson's ratio for ductile materials is larger than 0.26, while the value of brittle materials is less than 0.26.[74] For binary Hf–Rh intermetallics, they are all ductile materials (Table 3). The hardest $HfRh_3$ phase has the Poisson's ratio of 0.282, while the comparatively softest compound of Hf_3Rh_4 owns a higher Poisson's ratio of 0.405. Poisson's ratio also provides useful information about the characteristic of bonding forces in solids.[75,76] The lower and upper limits for central force solids are 0.25 and 0.5, respectively. In this work, the Poisson's ratio for binary Hf–Rh compounds are larger than the lower limit 0.25, indicating that the interatomic forces in these intermetallics are all central forces.

The ratio of shear modulus to bulk modulus (B/G) has been proposed to estimate brittle or ductile behavior of materials.[77] A

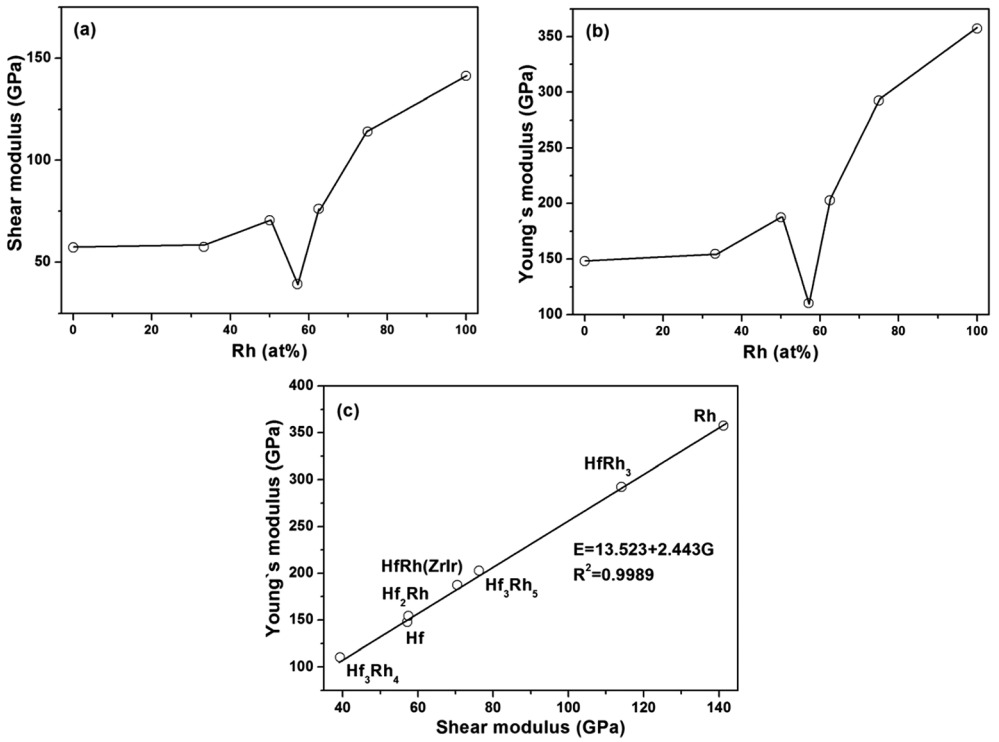

Fig. 3 The calculated (a) shear modulus (G) and (b) Young's modulus (E) *versus* Rh concentration (at%) for binary Hf–Rh compounds; (c) Young's modulus *versus* shear modulus for binary Hf–Rh intermetallics.

higher B/G ratio is associated with the better ductility, whereas a lower value corresponds to the naturally brittleness. The critical value which separates ductile from brittle material is 1.75. If $B/G > 1.75$, the material behaves in a ductile manner. Otherwise, the material behaves in a brittle manner. According to Table 3, all the binary Hf–Rh compounds are ascribed to

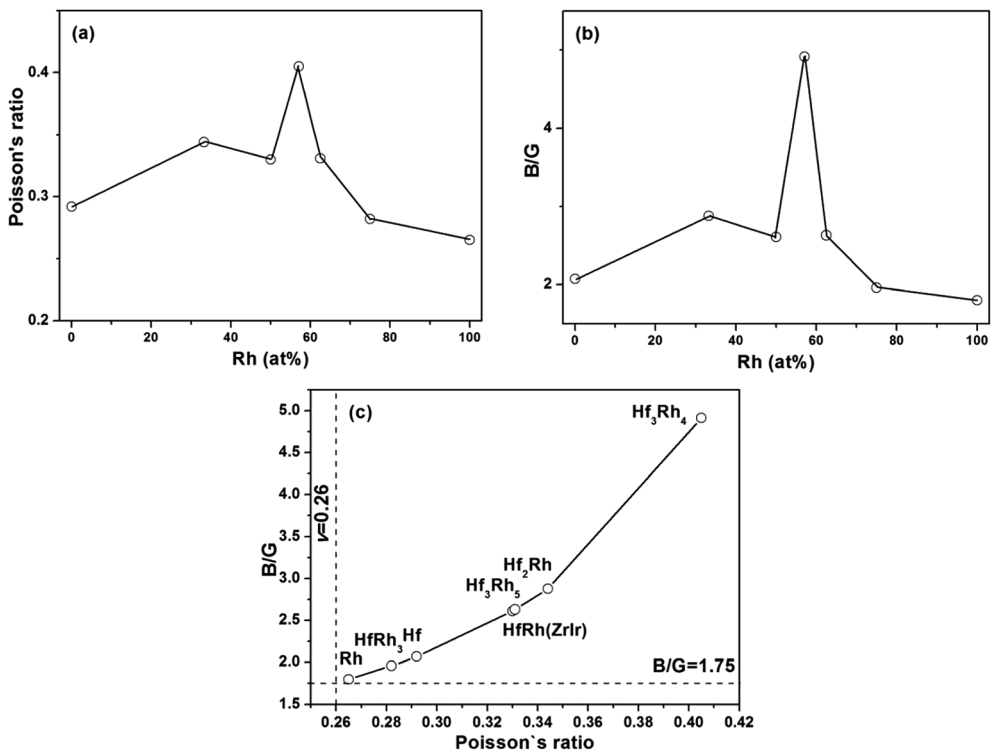

Fig. 4 The calculated (a) Poisson's ratio (ν) and (b) B/G ratio *versus* Rh concentration (at%) for binary Hf–Rh compounds; (c) Poisson's ratio *versus* B/G ratio for binary Hf–Rh intermetallics.

ductile materials, which agrees well with the prediction from the Poisson's ratio.

In the case that the ZrIr-HfRh is adopted, the variations of Poisson's ratio and B/G ratio have exhibited similar trends with the increasing Rh concentration from Fig. 4a and b, respectively. The relationship between Poisson's ratio and B/G ratio are shown in Fig. 4c. It has further confirmed the ductile essence of binary Hf–Rh compounds, and found the compound with a higher Poisson's ratio owns a higher B/G ratio simultaneously.

3.3 Density of states

In this work, the calculated electronic structure is helpful to get an insight into the bonding characteristics of binary Hf–Rh

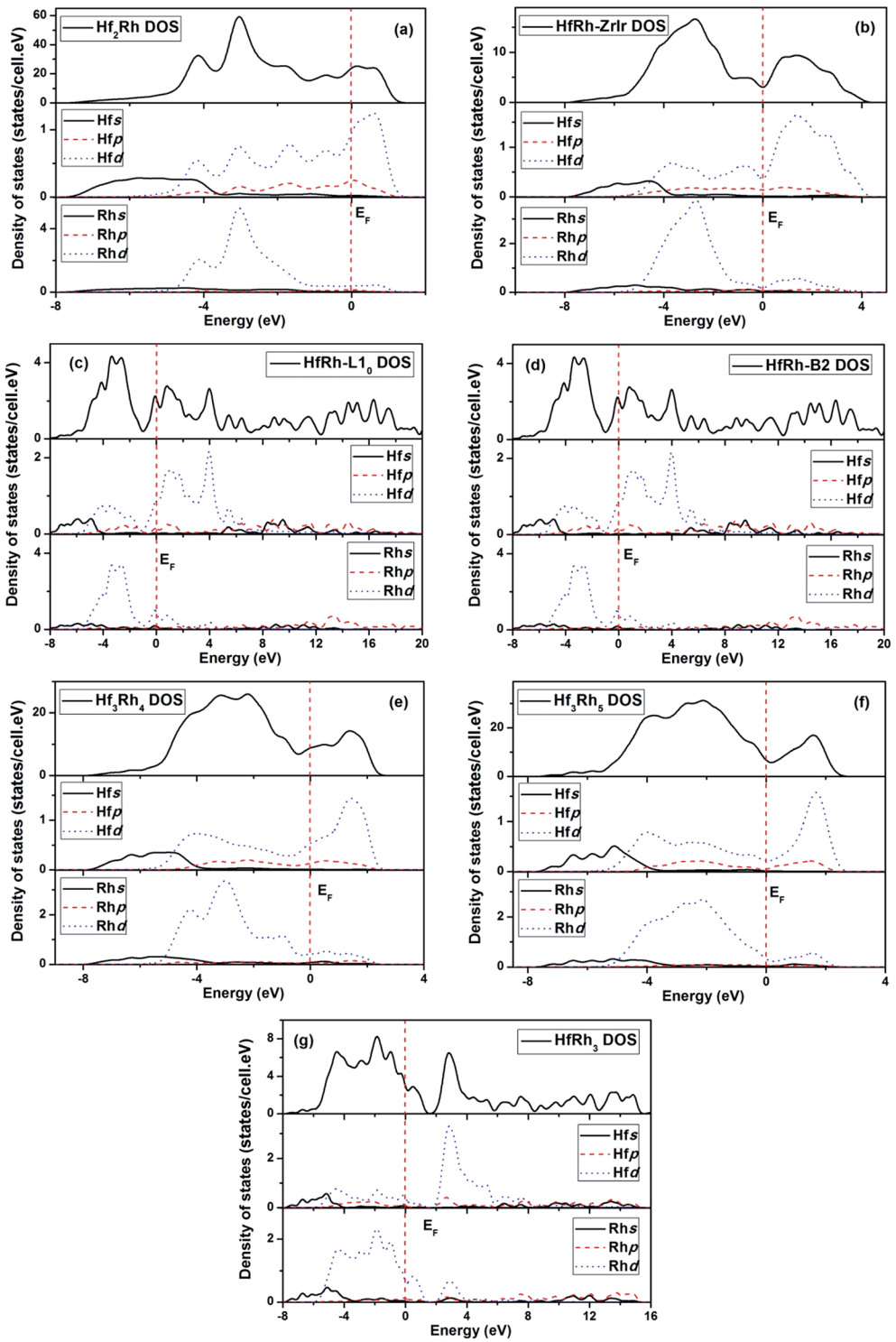

Fig. 5 Total and partial density of states for (a) Hf_2Rh, (b) ZrIr-HfRh, (c) $L1_0$-HfRh, (d) B2-HfRh, (e) Hf_3Rh_4, (f) Hf_3Rh_5 and (g) $HfRh_3$ compounds.

compounds, and to reveal the underlying mechanism of structural stability. In Fig. 5a–g, the theoretically calculated total and partial density of states (DOS) for the seven compounds in the Hf–Rh system, where the zero energy in each plotted figure corresponds to Fermi level (E_F). Based on the histogram curves, some common features can be identified in these compounds. For example, the peaks of the bonding state below Fermi level are mainly due to the hybridization between Rhd and Hfd electrons in the TDOS. While, the peaks of the antibonding state above the Fermi level are mainly due to the corresponding Hfd electrons. The s electrons of Rh and Hf can make the dominant contributions at deep levels between -8 and ~ -3 eV below the Fermi level. Additionally, The p electrons of Hf are effective around Fermi level in both bonding and antibonding states, and the p electrons of Rh are merely active. Similar featuring properties are identified in TDOS of Zr–Rh system.[45] Furthermore, the nonzero TDOS at the Fermi level has symbolized the Hf–Rh system as the metallic material.

The DOS curves of ZrIr-HfRh, $L1_0$-HfRh and B2-HfRh are compared in Fig. 5b, c and d, correspondingly. In Fig. 5b, the E_F falls exactly on the pseudogap for the TDOS of ZrIr-HfRh structure, indicating its superb stability.[78] In comparison, the $L1_0$-HfRh and B2-HfRh structures have very similar TDOS profiles, where the Fermi levels are locating at the peaks approaching to the antibonding states. These features have confirmed the conclusion that the ZrIr-HfRh compound is more stable at the ground state.

In order to evaluate the structural stability of the HfRh compounds, the number of bonding electrons per atom is calculated based on the TDOS spectra. Since the charge interaction among bonding atoms is very crucial to the material's stability, the compound possesses higher number of bonding electrons should be more stable structurally.[79–81] For the ZrIr-, $L1_0$- and B2-HfRh phases, the number of bonding electrons per atom of ZrIr-, $L1_0$- and B2- are 6.4974, 6.4943 and 6.494, accordingly. It means the HfRh phases has the stability order of ZrIr-type > $L1_0$ > B2, which is in good accordance with the thermodynamic analysis from Table 1. Additionally, for Hf_2Rh, ZrIr-HfRh, Hf_3Rh_4, Hf_3Rh_5 and $HfRh_3$, the calculated number of bonding electrons per atom have the results of 5.6594, 6.4974, 6.8527, 7.122 and 6.2456 accordingly. Therefore, the sequence of structural stability of the five stable Hf–Rh intermetallics should be Hf_3Rh_5 > Hf_3Rh_4 > ZrIr-HfRh > $HfRh_3$ > Hf_2Rh. This conclusion is in consistency with the conclusion drawn from formation enthalpies for five intermetallics, as shown in Fig. 1.

4. Conclusions

The phase stability, elastic and electronic properties of binary Hf–Rh compounds have been investigated using first-principles calculations. There are several conclusions are drawn as following:

(1) Based on the formation enthalpy analysis, the equiatomic HfRh phase should tend to crystallize in ZrIr-type structure, followed by $L1_0$, and then B2 at the ground state. Therefore, the lower temperature HfRh phase is suggested to be the ZrIr-type. This conclusion is in good agreement with the experimental reports in the literature. Besides, Hf_3Rh_4 is proposed to be Pu_3Pd_4-type for the first time.

(2) There are seven compounds (*i.e.*, Hf_2Rh, ZrIr-HfRh, $L1_0$-HfRh, B2-HfRh, Hf_3Rh_4, Hf_3Rh_5, and $HfRh_3$) are considered. The optimized lattice constants show a good consistency with available results. Furthermore, Hf_3Rh_5 is the most stable with the lowest formation enthalpy among the binary Hf–Rh compounds.

(3) The calculated elastic constants for Hf_2Rh, ZrIr-HfRh, $L1_0$-HfRh, B2-HfRh, Hf_3Rh_4, and Hf_3Rh_5 can all satisfy the Born's criteria, indicating their mechanical stabilities.

(4) The elastic modulus of the compound is calculated using the VRH method. When ZrIr-HfRh is considered, the bulk modulus (B) increases linearly with the growing Rh concentration. Besides, it is found Young's modulus has linearly increased with the growing shear modulus, and the compound with a higher Poisson's ratio owns a higher B/G ratio simultaneously. Overall, the analysis made on the Poisson's ratio and B/G ratio have indicated that all the considered Hf–Rh compounds should be ductile.

(5) The number of bonding electrons for each compound has been derived from the DOS analysis. The results show the sequence of structural stability should be Hf_3Rh > Hf_3Rh_4 > ZrIr-HfRh > $HfRh_3$ > Hf_2Rh, which is in remarkable agreement with the thermodynamic analysis.

Acknowledgements

This work is sponsored by Research Fund (Project No. 12X100030002 and No. 15X100040018) at Shanghai Jiao Tong University, P. R. China.

References

1 Y. Yamabe-Mitarai, Y. Koizumi, H. Murakami, T. Maruko, Y. Ro and H. Harada, *Scr. Mater.*, 1997, **36**, 393.
2 P. M. Clark, S. Lee and D. C. Fredrickson, *J. Solid State Chem.*, 2005, **178**, 1269.
3 *ASM handbook*, ed. S. D. Cramer and B. S. Covino, 10th edn, vol. 13B, ASM International, Metals Park (OH), 2005.
4 K. Chen, L. R. Zhao, J. S. Tse and J. R. Rodgers, *Phys. Lett. A*, 2004, **331**, 400.
5 G. Surucu, K. Colakoglu, E. Deligoz, N. Korozlu and H. Ozisik, *Comput. Mater. Sci.*, 2010, **48**, 859.
6 Y. Terada, K. Ohkubo, S. Miura, J. M. Sanchez and T. Mohri, *J. Alloys Compd.*, 2003, **354**, 202.
7 R. Kuentzler and R. M. Waterstrat, *Solid State Commun.*, 1988, **68**, 85.
8 Y. Mao and Y. Q. Gao, *J. Non-Cryst. Solids*, 1988, **105**, 134.
9 J. Belosevic-Cavor, B. Cekic, V. Koteski and A. Umicevic, *Mater. Sci. Eng., A*, 2007, **462**, 294.
10 R. M. Waterstrat and A. A. Giuseppetti, *J. Less-Common Met.*, 1986, **119**, 327.
11 V. N. Eremenko, T. D. Shtepa, T. A. Velikanova, L. S. Krikiya and V. M. Petyukh, *Izv. Akad. Nauk SSSR, Met.*, 1991, **6**, 143.
12 M. V. Nevitt and L. H. Schwartz, *Trans. Metall. Soc. AIME*, 1958, **212**, 700.

13 A. E. Dwight, *Trans. Metall. Soc. AIME*, 1959, **215**, 283.
14 A. Ramam and K. Schubert, *Z. Metallkd.*, 1964, **55**, 704.
15 V. N. Eremenko, T. D. Shtepa and T. A. Velikanova, *Dokl. Akad. Nauk Ukr. SSR, Ser. B: Geol., Khim. Biol. Nauki*, 1985, **10**, 72.
16 H. Okamoto, *J. Phase Equilib.*, 1993, **14**, 399.
17 M. D. Segall, P. J. D. Lindan, M. J. Probert, C. J. Pickard, P. J. Hasnip, S. J. Clark and M. C. Payne, *J. Phys.: Condens. Matter*, 2002, **14**, 2717.
18 D. Vanderbilt, *Phys. Rev. B: Condens. Matter Mater. Phys.*, 1990, **41**, 7892.
19 J. P. Perdew and Y. Wang, *Phys. Rev. B: Condens. Matter Mater. Phys.*, 1992, **45**, 13244.
20 J. P. Perdew, K. Burke and M. Ernzerhof, *Phys. Rev. Lett.*, 1996, **77**, 3865.
21 M. Ernzerhof and G. E. Scuseria, *J. Chem. Phys.*, 1999, **110**, 5029.
22 H. J. Monkhorst and J. D. Pack, *Phys. Rev. B: Solid State*, 1976, **13**, 5188.
23 P. Pulay, *J. Chem. Phys.*, 1983, **78**, 5043.
24 B. Hammer, L. B. Hansen and J. K. Nørskov, *Phys. Rev. B: Condens. Matter Mater. Phys.*, 1999, **59**, 7413.
25 D. F. Shanno, *Math. Comput.*, 1970, **24**, 647.
26 P. E. Blöchl, O. Jepsen and O. K. Andersen, *Phys. Rev. B: Condens. Matter Mater. Phys.*, 1994, **49**, 16223.
27 N. Ivanovic, S. Koicki, B. Cekic, M. Manasijevic, V. Koteski and D. Marjanovic, *J. Phys.: Condens. Matter*, 1999, **11**, 289.
28 Hf_3Rh_5, ICSD# 104267.
29 $HfRh_3$, ICSD #104266.
30 W. Xing, X. Q. Chen, D. Li, Y. Li, C. L. Fu, S. V. Meschel and X. Ding, *Intermetallics*, 2012, **28**, 16.
31 J. L. Jorda, T. Graf, L. Schellenberg, J. Muller, K. Cenzual, J. C. Gachon and J. Hertz, *J. Less-Common Met.*, 1988, **136**, 313.
32 E. L. Semenova and Y. V. Kudryavtsev, *J. Alloys Compd.*, 1994, **203**, 165.
33 R. M. Waterstrat, J. K. Stalick, X. Meng-Burany and M. A. Estermann, *Scr. Metall. Mater.*, 1995, **33**, 695.
34 J. K. Stalick and R. M. Waterstrat, *J. Alloys Compd.*, 2009, **477**, 123.
35 B. S. Chen, Y. Z. Li, X. Y. Guan, C. Wang, C. X. Wang and Z. Y. Gao, *Comput. Mater. Sci.*, 2015, **105**, 66.
36 W. Z. Chen, Z. Y. Jiang, L. Si, L. S. Li and B. Zhou, *Solid State Commun.*, 2011, **151**, 1433.
37 S. M. Shapiro, G. Xu, G. Gu, J. Gardner and R. W. Fonda, *Phys. Rev. B: Condens. Matter Mater. Phys.*, 2006, **73**, 214114.
38 M. Y. Benarchid, N. David, J. M. Fiorani, M. Vilasi and T. Benlaharche, *Thermochim. Acta*, 2009, **482**, 39.
39 Y. Yamabe-Mitarai, T. Hara, M. J. Phasha, E. Ngoepe and H. K. Chikwanda, *Intermetallics*, 2012, **31**, 26.
40 P. Shao, L. P. Ding, D. B. Luo, J. T. Cai, C. Lu and X. F. Huang, *J. Alloys Compd.*, 2017, **695**, 3024.
41 B. H. Chen and H. F. Franzen, *J. Less-Common Met.*, 1999, **153**, L13.
42 J. Li, M. Zhang and X. Luo, *J. Alloys Compd.*, 2013, **556**, 214.
43 C. Colinet, *Intermetallics*, 2003, **11**, 1095.
44 O. Levy, G. L. W. Hart and S. Curtarolo, *Acta Mater.*, 2010, **58**, 2887.
45 S. Zhang, X. Zhang, Y. Zhu, S. Zhang, L. Qi and R. Liu, *Intermetallics*, 2014, **44**, 31.
46 V. Koteski, J. Belosevic-Cavor, B. Cekic, D. Stojic, N. Simic, A. Umicevic and Z. Milosevic, *J. Alloys Compd.*, 2007, **442**, 252.
47 HfRh, ICSD# 104265.
48 N. Novaković, N. Ivanović, V. Koteski, I. Radisavljević, J. Belošević-Čavor and B. Cekić, *Intermetallics*, 2006, **14**, 1403.
49 Q. Guo and O. J. Kleppa, *J. Alloys Compd.*, 2001, **321**, 169.
50 A. Dębski, *Arch. Metall. Mater.*, 2013, **58**, 1147.
51 J. C. Gachon, N. Selhaoui, B. Aba and J. Hertz, *J. Phase Equilib.*, 1992, **13**, 506.
52 W. J. Ding, J. X. Yi, P. Chen, D. L. Li, L. M. Peng and B. Y. Tang, *Solid State Sci.*, 2012, **14**, 555.
53 G. V. Sin'ko, *Phys. Rev. B: Condens. Matter Mater. Phys.*, 2008, **77**, 104118.
54 Y. H. Duan, B. Huang, Y. Sun, M. J. Peng and S. G. Zhou, *J. Alloys Compd.*, 2014, **590**, 50.
55 Q. Chen and B. Sundman, *Acta Mater.*, 2001, **49**, 947.
56 N. Singh, *Pramana*, 1999, **52**, 511.
57 M. Born and K. Huang, *Dynamical Theory of Crystal Lattices, Oxford*, Oxford University Press, 1954.
58 D. Shi, B. Wen, R. Melnik, S. Yao and T. Li, *J. Solid State Chem.*, 2009, **182**, 2664.
59 D. Chen, Z. Chen, Y. Wu, M. Wang, N. Ma and H. Wang, *Comput. Mater. Sci.*, 2014, **91**, 165.
60 J. Du, B. Wen, R. Melnik and Y. Kawazoe, *J. Alloys Compd.*, 2014, **588**, 96.
61 Q. J. Liu, H. Qin, Z. Jiao, F. S. Liu and Z. T. Liu, *Mater. Chem. Phys.*, 2016, **180**, 75.
62 Y. H. Duan, Z. Y. Wu, B. Huang and S. Chen, *Comput. Mater. Sci.*, 2015, **110**, 10.
63 X. Gao, Y. Jiang, R. Zhou and J. Feng, *J. Alloys Compd.*, 2014, **587**, 819.
64 S. Chen, Y. H. Duan, B. Huang and W. C. Hu, *Philos. Mag.*, 2015, **95**, 3535.
65 H. Ozisik, E. Deligoz, K. Colakoglu and G. Surucu, *Chin. Phys. B*, 2013, **22**, 046202.
66 W. Voigt, *Lehrbuchde Kristallphysik*, Terubner, Leipzig, 1928.
67 A. Reuss, *Z. Angew. Math. Mech.*, 1929, **9**, 49.
68 R. Hill, *Proc. Phys. Soc., London, Sect. A*, 1952, **65**, 349.
69 B. Huang, Y. H. Duan, W. C. Hu, Y. Sun and S. Chen, *Ceram. Interfaces*, 2015, **41**, 6831.
70 M. Rajagopalan and M. Sundareswari, *J. Alloys Compd.*, 2004, **379**, 8.
71 B. Mayer, H. Anton, E. Bott, M. Methfessel, J. Sticht, J. Harris and P. C. Schmidt, *Intermetallics*, 2003, **11**, 23.
72 M. Pang, Y. Zhan, H. Wang, W. Jiang and Y. Du, *J. Appl. Phys.*, 2011, **110**, 033533.
73 G. N. Greaves, A. L. Greer, R. S. Lakes and T. Rouxel, *Nat. Mater.*, 2011, **10**, 823.
74 S. Chen, Y. Sun, Y. H. Duan, B. Huang and M. J. Peng, *J. Alloys Compd.*, 2015, **630**, 202.

75 D. Chen, Z. Chen, Y. Wu, M. Wang, N. Ma and H. Wang, *Intermetallics*, 2014, **52**, 64.
76 H. Fu, D. Li, F. Peng, T. Gao and X. Cheng, *Comput. Mater. Sci.*, 2008, **44**, 774.
77 S. F. Pugh, *Philos. Mag.*, 1954, **45**, 823.
78 S. Cui, W. Feng, H. Hu, Z. Feng and H. Liu, *Scr. Mater.*, 2009, **61**, 576.
79 W. C. Hu, Y. Liu, D. J. Li, X. Q. Zeng and C. S. Xu, *Comput. Mater. Sci.*, 2014, **83**, 27.
80 H. Hou, Z. Wen, Y. Zhao, L. Fu, N. Wang and P. Han, *Intermetallics*, 2014, **44**, 110.
81 W. C. Hu, Y. Liu, D. J. Li, X. Q. Zeng and C. S. Xu, *Phys. B*, 2013, **427**, 85.